Plasma Heating and Acceleration by Strong Magnetosonic Waves Propagating Obliquely to a Magnetostatic Field

B. Lembege[a] and J. M. Dawson
Department of Physics, University of California, Los Angeles, Los Angeles, California 90024
(Received 2 January 1984)

The behavior of strong magnetosonic waves with $\omega > \omega_{ci}$ ($\omega_{ci} = q_i B/m_i c$) is investigated in oblique propagation with particle simulation. Strong ion and electron heatings versus the angle [$\theta = (\vec{k}, \vec{B}_0)$] are found for $\theta < 90°$. Ion heating peaks at a particular angle but disappears below a critical angle θ_{t_i}; electron heating sets in below a second critical angle θ_{t_e}. The phenomena exhibit unexpected structure with θ.

PACS numbers: 52.50.Gj

Recent numerical studies[1] have shown that acceleration and heating of ions can be produced by intense magnetosonic waves propagating perpendicular to $\vec{B}_0$ for $\omega_{ci} < \omega < \omega_{1h}$. Here ω_{ci}, ω_{1h}, and ω are the ion-cyclotron, the lower-hybrid, and the pump-wave frequency, respectively. The basic processes can be summarized as follows: Let $\vec{B}_0 \| \vec{e}_z$ and $\vec{k} \| \vec{e}_x$. The initial response of electrons and ions to the strong magnetosonic wave is different and a large space-charge field E_{lx} develops. For intense waves this field can be strong enough to accelerate some ions to the phase velocity of the wave, v_ϕ, so that they become trapped in the potential troughs. While trapped, the $e(\vec{v}_\phi \times \vec{B}_z/c)$ force accelerates these ions parallel to the phase fronts (i.e., along the y axis). Ultimately, the Lorentz force [$e(\vec{v}_y \times \vec{B}_z/c)$] is larger than the accelerating force ($e\vec{E}_{lx}$), and the ions become untrapped and begin to gyrate around $\vec{B}_0$; this can produce particle velocities much larger than the phase velocity v_ϕ. Very strong heating of the ions (mainly nonstochastic) arises; the energy is absorbed at the expense of the wave and results in its strong damping. By contrast, the electrons are adiabatic and poorly heated.

Here we extend the investigation to the case when the angle between $\vec{k}$ and $\vec{B}_0$ is oblique [$\theta = (\vec{k}, \vec{B}_0)$]. Two main new results are found: (1) Strong ion heating and acceleration occur for $\theta_{t_i} < \theta \leq 90°$; (2) intense electron heating and acceleration occur for $\theta < \theta_{t_e}$, where θ_{t_i} and θ_{t_e} are two critical angles. Both effects show peaks and interesting structures as a function of θ.

The simulations were performed on a $1\frac{2}{2}$-dimensional, fully electromagnetic, relativistic particle code with both ions and electrons. A description of the code and of the dimensionless variables (denoted by a tilde) has been given in Ref. 1. Initially, a static external field $\vec{B}_0 = (B_{0x}, 0, B_{0z})$ is imposed and strong magnetosonic waves are generated by application of an external current (nonplasma current) $j_y = j_{0y} \sin(kx - \omega t)$. The wave number k is $k \equiv k_x = 2\pi m/L_x$, where m is the mode number and L_x is the length of the system. Similar results have been obtained for other m's but are not reported here. The frequency ω is determined from the Appleton-Hartree dispersion equation. Typical dispersion curves are shown in Fig. 1(a) for various values of θ; as shown by the circle points, for each θ, $\omega_{ci} \ll \omega < \omega_\theta$, where ω_θ is the asymptotic value reached by the dispersion curve.

In the simulations presented here, $\tilde{L}_x = 128$, and there were ten ions (i) and electrons (e) per grid spacing; initially $m_i/m_e = 100$ and $T_e/T_i = 1$; the electron thermal velocity at $\tilde{t} = 0$ is $\tilde{v}_{thx} = \tilde{v}_{thy} = \tilde{v}_{thz} = 1$; the light velocity is $\tilde{c} = 10$. The undisturbed magnetic field is $|\tilde{B}_0| = 5$. For these conditions, the gyrofrequency $\tilde{\omega}_c$, the plasma frequency $\tilde{\omega}_p$, the Larmor radius $\tilde{\rho}$, and the Debye length $\tilde{\lambda}_D$ are, respectively, for electrons, $\tilde{\omega}_{ce} = 0.5$, $\tilde{\omega}_{pe} = 1$, $\tilde{\rho}_e = 2$, $\tilde{\lambda}_{De} = 1$, and for ions, $\tilde{\omega}_{ci} = 0.005$, $\tilde{\omega}_{pi} = 0.1$, $\tilde{\rho}_i = 20$, $\tilde{\lambda}_{Di} = 0.1$. The ion gyroperiod is $\tilde{\tau}_{ci} \approx 1256$; the total run time is $\tilde{t}_{end} = 630$ so that $\tilde{t}_{end} \approx \tilde{\tau}_{ci}/2$. The characteristics of the applied current are $\tilde{j}_{0y} = 8$ and $\tilde{k}_x = 0.098\,17$.

The two reference coordinates (x,y,z) and ($\perp_2, \perp_1, \|$) are sketched in Fig. 1(b). For the sake of clarity, let us first consider separately the behavior of ions and electrons. From Fig. 1(a) by looking at the dispersion curves at the simulation points ($m = 2$, circle points) we see that the frequency (ω), the phase velocity ($v_{\phi x}$), and the group velocity (v_g) all increase as θ departs from 90°. However, the phase velocity parallel to $\vec{B}_0$, $v_{\phi\|} \simeq v_{\phi x} B_z/B_x$, decreases. For the following discussion, references should be made to Fig. 2. The higher phase velocity, $v_{\phi x}$, makes the ion trapping conditions ($v_{xi} \approx v_{\phi x}$) more stringent than for $\theta = 90°$; this implies stronger ion heating if they are trapped. The higher group velocity implies a more rapid transfer of energy to the wave for a given

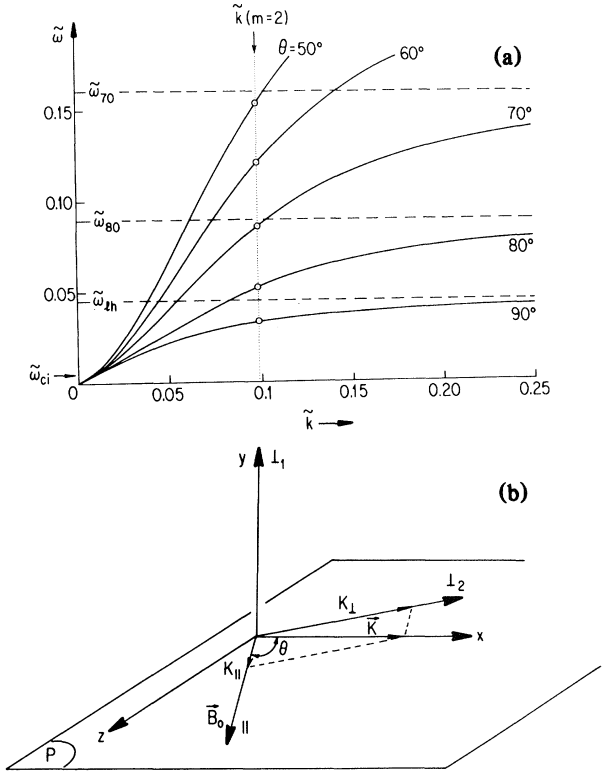

FIG. 1. (a) Dispersion curves $(\tilde{\omega},\tilde{k})$ deduced from the solution of the Appleton-Hartree equation for various values of the angle $\theta=(\vec{k},\vec{B}_0)$. The plasma parameters are those mentioned in the text. The particular values $\tilde{\omega}_{80}$, $\tilde{\omega}_{70}$, etc., are the asymptotic values reached by the dispersion curves respectively defined by $\theta=80°$, 70°, etc. For $\theta=90°$, $\tilde{\omega}_{90}\equiv\tilde{\omega}_{lh}$. (b) Sketch of both reference sets (x,y,z) and $(\perp_2,\perp_1,\parallel)$. The vector $\vec{K}$ illustrates either the propagation wave vector $\vec{k}$, or the longitudinal electric field $\vec{E}_l$.

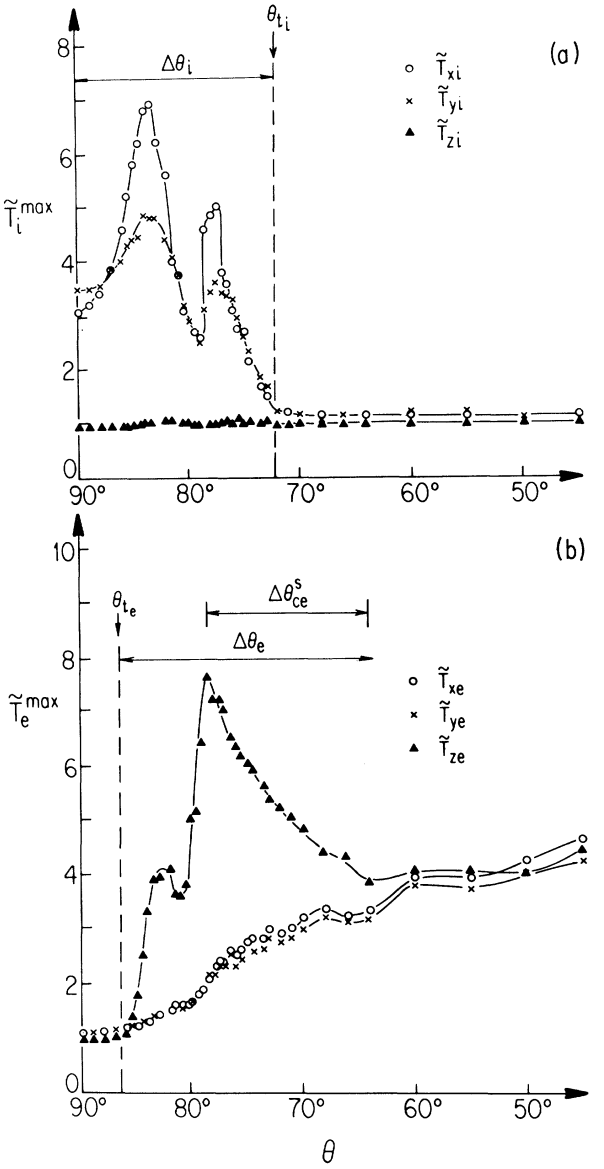

FIG. 2. Plots of the maximum values of the temperatures measured for the (a) ions and (b) electrons along the x, y, and z directions. These values are deduced from plots of local ion temperature vs time such as those of Fig. 3 of Ref. 1. Presently, the total length L_x of the model was divided into 16 boxes, each 8 grid points wide. Inside each box, the local temperature in direction α is estimated by calculating $\langle\tilde{p}_\alpha^2\rangle-\langle\tilde{p}_\alpha\rangle^2$ (averaged over all particles of a given kind in the box).

driving current which should give more rapid ion trapping. For the electrons the situation is different; as θ decreases the phase velocity parallel to $\vec{B}_0$ decreases and electrons are more strongly accelerated parallel to $\vec{B}_0$. Thus electrons can be accelerated to the phase velocity parallel to $\vec{B}_0$, and undergo wave trapping. This starts to occur for a critical angle $\theta<\theta_{t_e}$ when a few electrons begin to be trapped. As θ decreases, more and more electrons become trapped and the heating of the electrons increases. For a larger decrease of θ a point is reached where most of the electrons are trapped and the trapping energy is decreasing (because $v_{\phi\parallel}$ is decreasing). At this point the electrons to a large extent short out the E_{lx} field, which combined with the increasing $v_{\phi x}$ means that ion trapping is no longer possible; the ion heating disappears below a critical angle θ_{t_i}.

The development of the electron wave is graphically shown in phase space in Fig. 3 for the example $\theta=81°$ at times $\tilde{t}=0.07\tilde{\tau}_{ci}$, $0.19\tilde{\tau}_{ci}$, $0.26\tilde{\tau}_{ci}$, and $0.5\tilde{\tau}_{ci}$, respectively, for cases (a)–(d); each point is the position $\tilde{x}$ and parallel momentum $\tilde{p}_{\parallel e}$ of an electron. The characteristic features of electron trapping are clearly apparent. For the case where

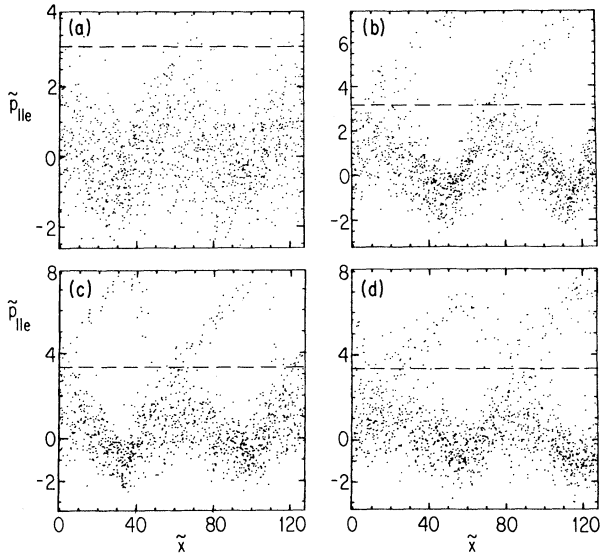

FIG. 3. Electron phase-space plots $(\tilde{x},\tilde{p}_{\|e})$ at times (a) $\tilde{t}=90$, (b) 240, (c) 330, and (d) 630 for the case $\theta=81°$. The dashed line represents the parallel phase momentum value $\tilde{p}_{\phi\|}$ of the wave $\{\tilde{p}_{\phi\|}=\tilde{v}_{\phi\|}/[1-(\tilde{v}_{\phi\|}/\tilde{c})^2]^{1/2}=3.35$, where $\tilde{v}_{\phi\|}=\tilde{\omega}/\tilde{k}_{\|}\}$.

the parallel phase velocity is near the initial electron thermal velocity ($\tilde{p}_{\phi\|}/\tilde{p}_{the}\simeq 3.33$, where $\tilde{p}_{\phi\|}$ is represented by a dashed line in Fig. 3), electron trapping occurs early in time [$\tilde{t}=90$ in Fig. 3(a)]. The earlier that trapping occurs the greater is the trapped electron density, since the growing wave continuously feeds accelerated electrons to the parallel phase momentum $\tilde{p}_{\phi\|}$, as shown in Figs. 3(a)–3(d). Two interesting features which are quite different from the ion behavior have to be noticed. First, since this trapping effect occurs along the direction parallel to $\vec{B}_0$ as a result of the component $E_{l\|}$ of the electrostatic field, there is no acceleration along the y direction as a result of the $\vec{E}\times\vec{B}$ drift [see Fig. 1(b)]; consequently no electron detrapping by the magnetic force similar to that involved with the ions occurs. Second, we recover the characteristic vortex structure of trapped particles observed in phase space for unmagnetized plasma since presently the electrons which move along $\vec{B}_0$ ignore the presence of this field. The trapped electrons largely overshoot the parallel phase momentum $\tilde{p}_{\phi\|}$ so that the apex of the loop is at $\tilde{p}_{\|e}\approx 2\tilde{p}_{\phi\|}$ at later times as shown in Fig. 3(d).

The behavior of the distribution functions for each species of particle is illustrated at the time $\tilde{t}=\tilde{\tau}_{ci}/2$ in Fig. 4; the solid and the dotted lines are respectively for the parallel ($p_{\|}$) and perpendicular ($p_{\perp_2}$) momentum. For the ions, we recover results

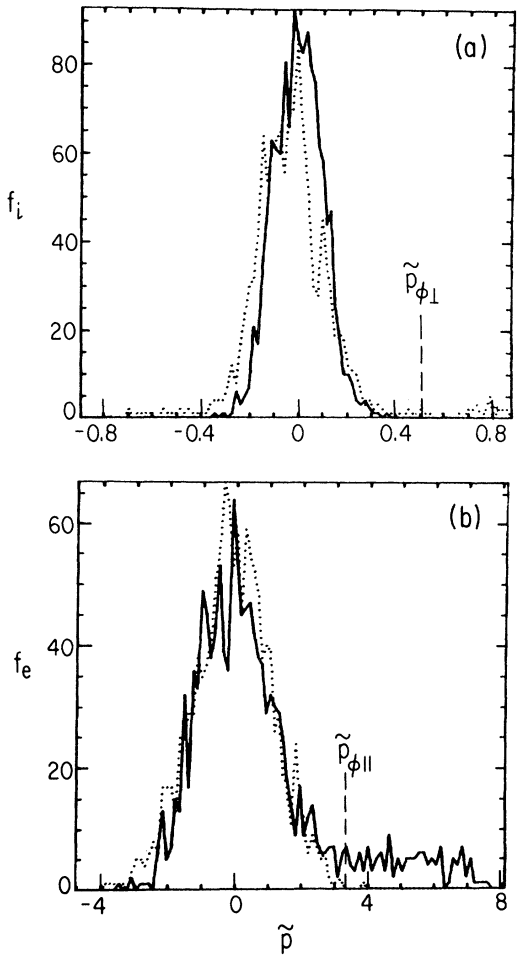

FIG. 4. Distribution of (a) ions and (b) electrons at the time $\tilde{t}=630$ for $\theta=81°$; the solid and dotted curves are used respectively for the parallel momentum $\tilde{p}_{\|}$ and perpendicular momentum $\tilde{p}_{\perp_2}$ of the particles.

similar to those observed for $\theta=90°$, i.e., presently a drift of particles with $p_{\perp_2 i}>0$ for early times and the formation of energetic ion tails in both $f(p_{\perp_1 i})$ and $f(p_{\perp_2 i})$ for later times; no energetic ion motion is observed along $\vec{B}_0$ [Fig. 4(a)]. The corresponding heating and gyration effects are observed in the plots of the temperature $\tilde{T}_{\perp_1 i}$ and $\tilde{T}_{\perp_2 i}$ such as those of Fig. 3(a) of Ref. 1. However, new features are observed for the electrons. The trapping of electrons produces a strong acceleration of electrons along $\vec{B}_0$ which increases with time, since the amplitude of the electrostatic field E_l and correspondingly $E_{l\|}$ increases. We observe an important flat tail distribution in $f(p_{\|e})$ for $\tilde{p}_{\|e}>\tilde{p}_{\phi\|}$, which reflects the presence of a strong electron current along $\vec{B}_0$ [Fig. 4(b)] as well as heating (increase in

$\langle p^2 \rangle$).

The present results show that the increasingly intense wave continuously accelerates both ions and electrons from the bulk plasma into the corresponding trapped regions, respectively controlled by the components $E_{l\perp_2}$ and $E_{l\parallel}$ of the electrostatic field E_l. Ultimately the drive is unable to sustain the wave against the increasing dissipation and a rapid damping sets in (not shown). It is important to determine how the dissipated energy of the wave is distributed between the electrons and ions as well as which components of the momentum $(p_\parallel, p_\perp)$ are affected. For this, we investigate the variation, versus the angle θ, of the maximum values of the temperatures attained by both ions and electrons with regard to the x, y, and z axis. Plots of $\tilde{T}_i^{\max}$ and $\tilde{T}_e^{\max}$ are shown respectively in Figs. 2(a) and 2(b).

For the ions, we see clearly that strong heating still exists for an angular range $\Delta\theta_i$; in fact it can be much larger than for $\theta = 90°$. The size of $\Delta\theta_i$ fits quite well with the picture that ion trapping becomes harder as the deviation from 90° increases and the electron shorting of the longitudinal field E_l becomes more effective. For $\theta > \theta_{t_i}$, a large-scale modulation is observed in both curves $\tilde{T}_{xi}^{\max}$ and $\tilde{T}_{yi}^{\max}$; calculations not reported here indicate that this modulation is strongly related to the electron behavior.

For the electrons, very efficient heating is observed along the three axes when θ is oblique and becomes particularly large along the z axis within a certain angular range $\Delta\theta_e$ different from $\Delta\theta_i$; it reflects quite well the strong heating expected along $\vec{B}_0$ (i.e., $T_{\parallel e} \approx T_{ze}$) since $T_{ze} >> T_{xe}$ within this range [Fig. 2(b)]. The electron heating starts only from a critical angle which agrees well with the value θ_{t_e} at which electron trapping becomes important ($eE_{l\parallel}/m_e\omega \approx v_{\phi\parallel}$). It is important to note that for lower values of θ (θ below $\Delta\theta_e$), reasonable electron heating is still present because electron trapping continues while the ion heating vanishes completely for $\theta < \theta_{t_i}$.

The presence of a single critical angle for which the particle velocity v_z exhibits a maximum value has been recently considered.[2] Although some similarities appear qualitatively with our results of Fig. 2, a direct comparison cannot be made, since Ref. 2 does not include mass ratio and self-consistent effects. Both effects are essential in the present study since they define the number of peaks in the curves of Fig. 2; additionally the location of these peaks is quite different according to the particle species of concern, which does not occur in Ref. 2.

In summary, the present results show that a strong acceleration and heating of both electrons and ions occur in the presence of strong magnetosonic waves when the angle $\theta = (\vec{k}, \vec{B}_0)$ is oblique. The electron heating mechanism is particularly large along the direction parallel to $\vec{B}_0$ while that for the ions is strong within the plane $(\perp_2, \perp_1)$ perpendicular to $\vec{B}_0$; only ion heating occurs in the particular case $\theta = \pi/2$. Both phenomena are governed by the trapping and untrapping conditions of the different kinds of particles, i.e., by the sets of coupled values $(\omega, k_\parallel, E_{l\parallel})$ for the electrons and $(\omega, k_{\perp_2}, E_{l\perp_2})$ for the ions. The two trapping conditions vary strongly with angle θ; ion trapping dominates around 90° and electron trapping for smaller angles. There is an intermediate angular range where both processes occur and this gives rise to detailed structure in the heating curves (Fig. 2).

It is of interest that the dissipation mechanisms discussed here apply to a broad range of frequencies where no resonance is involved ($\omega_{ci} << \omega < \omega_\theta$) as illustrated in Fig. 1(a). These mechanisms can be invoked to heat plasmas in fusion systems or in many space plasma phenomena; either ions or electrons or both can be heated. In this paper, because of the lack of space we have restricted the treatment to a qualitative discussion of what turned out to be a more complex and richer problem than one would expect. The qualitative arguments can be made quantititative and this will be done in a further, more extensive paper which will also report a wider parametric study.

We would like to thank Jean-Noël LeBoeuf for helpful discussions and Chih-Chien Lin for supplying the computer code. This work was supported by the U. S. Department of Energy under Contract No. DE-AMD3-SF7600010 PA 26, Task VIB.

---

[a]On leave from the Centre de Recherches en Physique de l'Environnement Terrestre et Planetaire, Centre National d'Etudes des Telécommunications, F-92131 Issy Les Moulineaux, France.

[1]B. Lembege, S. T. Ratliff, J. M. Dawson, and Y.Ohsawa, Phys. Rev. Lett. **51**, 264 (1983).

[2]R. Sugihara, S. Takeuchi, K. Sakai, and M. Matsumoto, Phys. Rev. Lett. **52**, 1500 (1984).